Hindawi
Advances in Civil Engineering
Volume 2019, Article ID 8151087, 17 pages
https://doi.org/10.1155/2019/8151087

Research Article

Experimental Study on Novel Energy-Dissipating Prefabricated Beam-Column Joints

Qiong Liu, Shanghong Chen, Wei Lin, and Fanjin Zeng

College of Civil Engineering, Fuzhou University, Fuzhou 350108, China

Correspondence should be addressed to Shanghong Chen; chenshanghong@fzu.edu.cn

Received 16 August 2019; Revised 4 December 2019; Accepted 5 December 2019; Published 23 December 2019

Academic Editor: Huu-Tai Thai

A new dapped-end beam to column connection is designed in this paper. Its assembly connection zone changes from inside the joint to midspan of the beam. The proposed connection can not only provide good structural integrity but also ensure that the plastic hinge moves away from the column edge. The rotational capacity of the plastic hinge determines the internal force redistribution of the joint and the energy dissipation capacity. The high-strength bolts and steel plates are used to realize connection, further enhancing the rotation of the plastic hinge and minimizing the cast-in-place concrete volume. Three full-scale exterior beam to column joints are casted and then subjected to reversal cyclic loading. The finite element (FE) analyses are carried out to compare with experimental results and study the effect of connection position on the structural behaviours. The obtained results show that the plastic hinges of all three specimens are firstly developed to a distance from the column edge, thus revealing that this kind of joint can achieve beam hinge mechanism and prevent joint shear failure. And the connection position is the most disadvantaged when coinciding with the plastic hinge zone, which would result in the excessive deformation and the early failure of the steel bar anchor system. The new type of joint shows good seismic performance during earthquake if the connection can be properly designed, and thus this kind of structural form can be applied to actual engineering structures in seismic regions.

1. Introduction

Currently, fabricated buildings are promoted actively because of their faster construction speed, better quality control, and environmentally friendly technology [1]. Beam-column joints are acted as the weakest transmission links in prefabricated frames because shear forces are transmitted through joint and high shear forces are mainly concentrated in the joint core area under strong earthquake excitations. The postsevere damage of building structures is mainly attributed to the failure of beam to column joint. Thus, the transmission properties and the integrity of joints play an important role in the safety of precast buildings [2].

In order to ensure adequate joint strength, different types of beam-column joints are proposed. Prefabricated monolithic joints with keyseats are designed, and experimental results show that the reasonable joint design and the appropriate cast-in-site concrete volume can make prefabricated joints equivalent to monolithic joints. This kind of connection is efficient to improve the seismic behaviour in the high seismic intensity zones [3, 4]. But the large volume of cast-in-place concrete may nullify advantages of this kind of joint. This means that cast-in-place monolithic joints cannot facilitate resource saving and friendly environment. Priestley carried out dynamic time history analyses of precast prestressed beam-column joints with unbonded tendons. Results showed that unbonded tendons can provide good structural integrity and auto-recovery ability for the joint, but the use of prestressed tendons would make the ductility and the energy dissipation capacity of this type of joint very poor [5–7]. This problem is easy to scientific scholars who have devoted great efforts to propose energy dissipation dampers, which can be attached to the column and beam ends. The friction dampers are used in the prestressed beam-column joints to assume energy, and unbonded tendons are used to provide self-centering capacity for joints [8–10]. The poor energy dissipation capacity of the precast prestressed beam-column joints limits their

spreading use, but the use of additional energy dissipation dampers can help to absorb energy; nevertheless, the dampers would interfere with other components of the frame.

In the new beam-column joint system, prefabricated columns are cast continuously with a free space in the connection zone to connect the U-shaped beam shell. This kind of joint can provide good structural intergrety in the connection zone. [11–13]. But the shear strength of joints drops due to the reduced column depth in the joint, which means that this kind of joint cannot achieve the strong-joint weak-component failure mechanism. To face this problem, researchers have proposed alternative methods that can provide good protection for joints. It is well known that the position of the plastic hinge has significant effects on the mechanical performance of joints. Chio et al. proposed a new type of joint, and its U-shaped cross section beam and column were connected by steel plates in the core area. The plastic hinge zone was relocated away from the column edge by taking advantage of the deformation of the steel plates [14]. Furthermore, researchers have introduced other methods to transfer the plastic hinge zone from the column edge to beam span. As an alternative method to protect joint and relocate plastic hinge zones, the haunch systems which were made of steel bars and joint enlargement were used by Pampanin et al. [15] and Pimanmas and Chaimahawan [16]. Eom et al. also used two strengthening methods to achieve plastic hinge relocation such as hooked bars and headed bars. Except for strengthening methods, reducing beam bar section can also help to transfer plastic hinge zones to weakened beams [17]. In 2006, Chen et al. introduced an optimal method to improve ductility and promote the development of the plastic hinge. This means that the welding part of the beam-column joint was enhanced [18]. The plastic hinge moves from the column edge to the cutoff point of the CFRP, and specimens retrofitted by carbon fiber-reinforced polymer exhibit higher bearing capacity and ductility [19]. Although the above relocation form about the plastic hinge is a good way to avoid the shear failure of joints, the connection form constructed in the joint core area would disturb the continuity of longitudinal steel bars and the congested reinforcement in the joint would result in difficulty in concrete pouring. Considering that the flexural stiffness changes along the lap splice connection of the assembled beam and decreases at the transition section of the reduced profile, the connection position can be placed on the midspan of the beam [20]. Similarly, Astaneh-Asl also proposed that the semirigid connection can weaken the damage caused by seismic energy. In addition, the connection can be allowed to slip so that the earthquake energy can be absorbed through friction between contact surfaces [21]. Joshi and Patel conducted experimental studies on prefabricated connections which were constructed away from the junction area. The partial precast beam was connected to other prefabricated element through steel plates, and the prefabricated element was extended from the edge of the column. The test results showed that the proper precast connection design could ensure the same performance as monolithic specimens [22]. The short cantilever beam is casted as part of the precast column extending from the column edge. Another precast beam is connected to the cantilever beam through the lapping of the hooks [23, 24]. Previous studies verified that the seismic performance of prefabricated structures can be improved and meet the demand of seismic codes as long as the connections are properly designed and retrofitted for strength and ductility [25–27].

In this paper, experimental and numerical analyses of dapped-end beam to column joints are conducted. The work devotes to relocating the connection zone from the interior joint core area to midspan of the beam so as to achieve beam hinge mechanism. Another part of the precast beam is seated on the dapped-end cantilever beam and coupled to cantilever beam through high-strength bolts and steel plates, which can minimize the volume of cast-in-place concrete and get rid of additional strengthening or weakening systems.

2. Experiments on Joints

2.1. Specimen Design. Figure 1 describes the details of the proposed dapped-end cantilever beam to column joint. In the system, columns are prefabricated with continuous longitudinal bars in the joint in the same technology as conventional precast members. The cantilever beam with U-shaped groove is extended from the edge of column and another part of precast beam with corbel is seated on the cantilever beam. The U-shaped cross section groove is reserved at the end of the cantilever beam to make space for the corbel. Two precast members are connected through high-strength bolts. Considering the brittleness of concrete and small load-bearing areas of bolts on both sides of the U-shaped groove, two rigid steel plates are attached to the external surfaces of the U-shaped groove to distribute forces and avoid stress concentration. The length of the U-shaped groove is 150 mm same as the corbel but the height and the width are 300 mm and 200 mm larger than those of the corbel so that the connected cast-in-place space for concreting can be formed after anchorage of the corbel and the U-shaped groove. As a result, the cast-in-place concrete can provide integrity for the connection. The horizontal steel bars in the beam are reserved in the column and extended through the cantilever beam to the connection zone. Correspondingly, steel bars are extended from another part of the precast beam to the connection zone. These longitudinal steel bars at the bottom of the beam are connected by welding, and two longitudinal bars on the top of the beam and lateral longitudinal bars are connected by sleeves in the cast-in-place zone for concreting. In the installation process, the bolt shanks are used for position purpose so that the corbel can be seated on the U-shaped groove precisely.

In the installation process, the precast column is placed erectly and then another precast beam is seated on the cantilever beam. The bolt rods are used for the precise position to prevent assembly problem. After that, the horizontal steel bars on the top of the beam are bolted first, followed by the lateral bars. And the steel bars at the bottom of the beam are connected by welding. Then, the concrete is

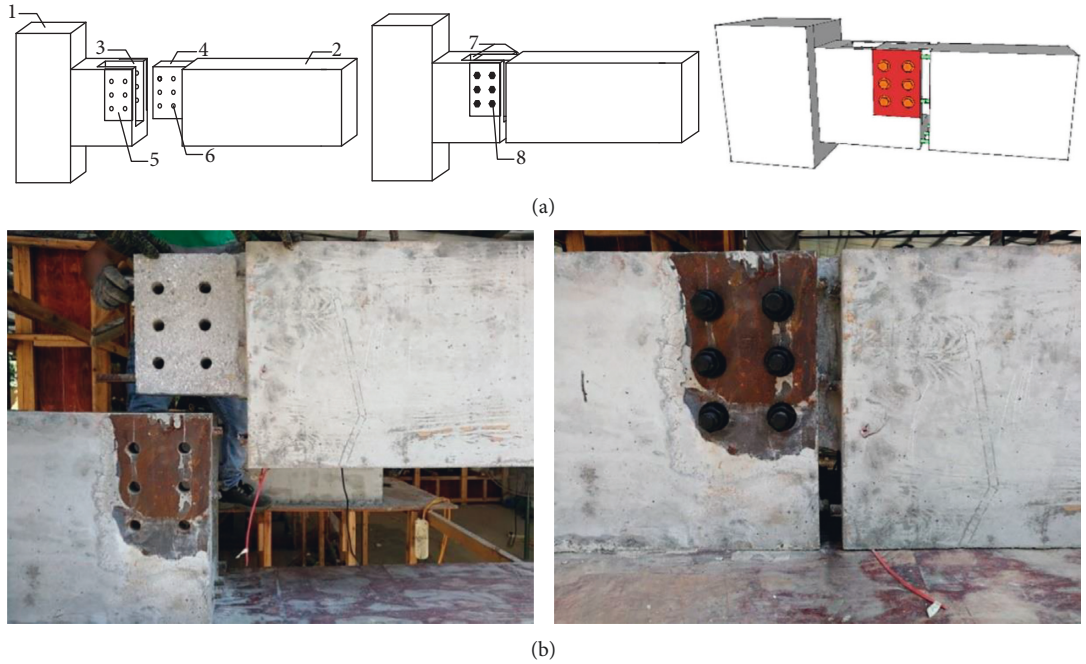

Figure 1: Beam-column joint details. (a) Design schematic diagram (1, column; 2, beam; 3, U-shaped groove; 4, corbel; 5, steel plate; 6, bolt hole; 7, cast-in-place area; 8, bolt). (b) Photo.

poured into the cast-in-place area to integrate the connection. Finally, the pretightening force is applied to the bolts.

The dapped-end beam to column joint can relocate the connection position from the joint core area to the beam span, which can provide the integrity for the joint. In this way, the plastic hinge can also be relocated away from the column edge so that the beam hinge mechanism can be achieved. Three types of joints PC1, PC2, and PC3 are designed to be 450 mm, 600 mm, and 750 mm away from the column edge, respectively. And it is known that the beam plastic hinge of precast joints is formed at a distance of about 1.0–1.3 times the height of the beam away from the column edge [17, 28]. As a result, the connection position of joints PC1 and PC2 coincides with the plastic hinge but the connection position of joint PC3 is away from the plastic hinge zone. The use of high-strength bolts and steel plates for connection can help to enhance the rotation of the plastic hinge, thus providing better deformation capacity.

Three full-scale exterior joints in frames (PC1, PC2, and PC3) were fabricated based on the design principles, having the seismic performance equivalent to cast-in-place joints. They were designed according to the *Chinese Standards of Detailing of Joints in Precast Concrete Structures* (15G310-1~2, 2015) [29] and *Technical Specification for Precast Concrete Structures* (JGJ 1-2014, 2014) [30]. Figure 2 shows the dimensions and reinforcement details in the joints with different connection positions, which were 450 mm, 600 mm, and 750 mm away from column edge, respectively. The column had a 400 × 400 mm cross section and a height of 2450 mm. The longitudinal reinforcements of each column included twelve D22 bars (C22). In order to improve the strength of the joint, the distance of the stirrups was designed to be 50 mm in the joint area. In other parts of the joint, the distance between the column stirrup was 100 mm. The beam had a 250 × 450 mm cross section and a length of 1500 mm. In the cantilever beam, within the distance of 300 mm away from the column edge and the corbel area in the precast beam, the distance of the stirrups was designed to be 50 mm. In other areas of the beam, the distance between the beam stirrup was 100 mm. The corbel was regarded as one of the main force elements, so a special steel bar frame was designed and embedded in the corbel area to ensure adequate bearing performance, which was made of concrete with D16 longitudinal steel bars (C16) of 400 mm and stirrups. All stirrups were D8 ordinary steel bars (A8). The concrete used in the specimens had a strength grade of C30 (nominal cubic compressive strength $f_{cu,d} = 30$ MPa and design axial compressive strength $f_{c,d} = 14.3$ MPa). High-strength bolts of grade 10.9 with the diameter of 24 mm and the length of 320 mm were used for assembling the joints.

2.2. Mechanical Analysis of Dapped-End Connection. It is essential for the dapped-end connection to transfer the shear force and the moment effectively. The force transfer system of the dapped-end connection under vertical load is shown in Figure 3. The four forces must be in equilibrium in both the horizontal and vertical directions. Vertical shear forces are transmitted to the core area of the joint by the U-shaped groove at the end of the cantilever beam and the corbel. Hence, the reliability of the connection mainly depends on the performance of the groove and the corbel. Assuming that the mutual friction between concrete interfaces has little influence on the force transfer mechanism, the full vertical

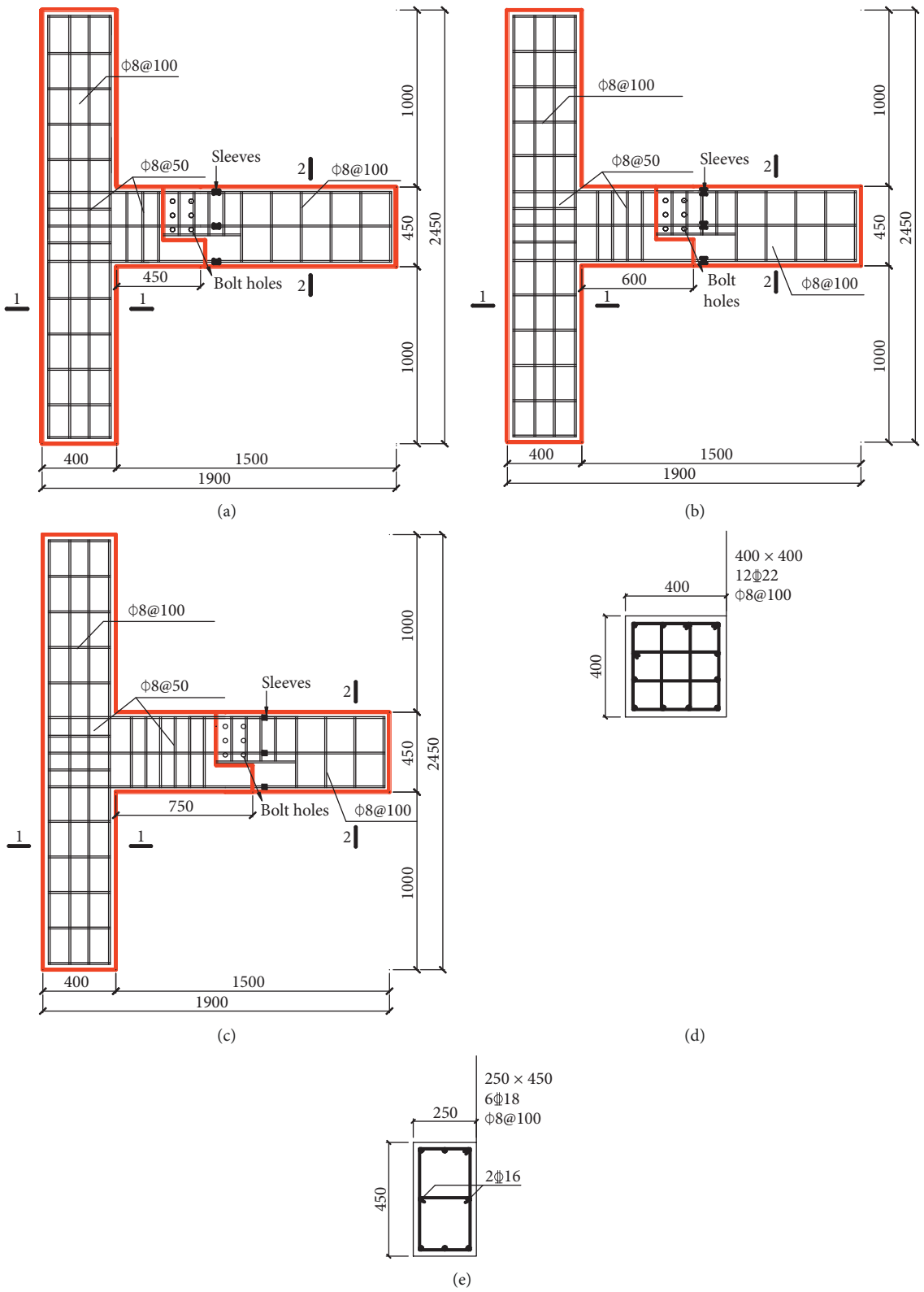

Figure 2: Dimensions and reinforcement details of PC1, PC2, and PC3. (a) Cross section of beam-column joint of PC1. (b) Cross section of beam-column joint of PC2. (c) Cross section of beam-column joint of PC3. (d) Column cross section. (e) Beam cross section (in mm).

shear force is sustained by the corbel. The U-shaped groove can be regarded as a reversed corbel, and thus its mechanical properties are similar to those of the corbel.

Based on the strut-and-tie model, the horizontal steel bars at the bottom of the corbel are regarded as the tie rod and internal compressed concrete is viewed as the diagonal

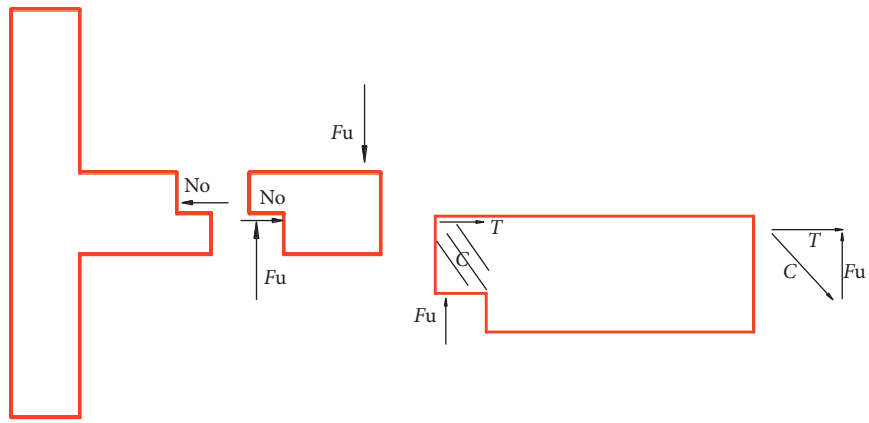

Figure 3: Calculation schematic.

struts. The force diagram of the corbel is shown in Figure 3, in which T is the tensile resistance of the steel bars, C is the compression force in the concrete, and F_u is the vertical bearing capacity obtained from equations (1)–(9).

$$C = A_{cx} f_{cx}, \tag{1}$$

where A_{cx} is the cross-sectional area of the end part perpendicular to small oblique blocks and f_{cx} is the effective concrete strength of the diagonal struts.

$$A_{cx} = \frac{\sqrt{2}}{2} bh, \tag{2}$$

$$f_{cx} = 0.85\beta_j f_c^0 = 0.85 \times 0.8 f_c^0, \tag{3}$$

where b and h are the width and the height of the corbel, respectively, and f_c^0 is the compression strength design value. Considering the effects of cracking development and multiaxial stress on the compressive strength of diagonal struts, the reduction ratio β_j of 0.8 is used to describe the strength reduction based on *American structure design code ACI Committee 318* [31].

$$Cl = A_{cx} f_{cx} = \frac{\sqrt{2}}{2} bh \times 0.85 \times 0.8 f_c^0, \tag{4}$$

$$T = f_y \times A_s, \tag{5}$$

$$F_u = T = \frac{\sqrt{2}}{2} C. \tag{6}$$

In order to ensure the safety of diagonal struts and the effectiveness of tie rods, the following formulas must be considered:

$$F_u \le 0.34 bh f_c^0, \tag{7}$$

$$\rho_s \le 0.34 \frac{f_c^0}{f_y}, \tag{8}$$

$$\rho_s = \frac{A_s}{bh}, \tag{9}$$

where ρ_s is the reinforcement ratio of tie bars and A_s is the maximum area of tie rods.

According to the above mechanical analysis, the strut-and-tie model has effects on the reliability of the corbel and the bearing capacity of the dapped-end connection. The reinforcement ratio of steel bars and compressive strength of diagonal struts both meet the design demands based on the above design parameters. This means that forces can be transmitted to the joint effectively.

2.3. Load Scheme. The axial force and the horizontal force were applied to the joints to simulate the axial load on the column caps and the lateral load from earthquake excitations, as shown in Figure 4. The horizontal force was applied by an actuator with 500 kN capacity, and the actuator was connected to the strong wall by a pin. The axial force was applied from the column top by a jack with 160 t capacity. The upper and lower ends of the column were hinged to effectively simulate the real boundary condition of the column. The bottom hinge was anchored to the ground and the upper hinge was attached to the reaction beam through a hydraulic jack. Two horizontal bracings were connected to the reaction wall to ensure the stability and safety of the specimen in the loading process.

During the loading test, the axial load was applied to the column by the hydraulic jack with a design axial compression ratio of 0.3 (801.6 kN). Considering the special structural configuration, it is hard to determine the accurate yield displacement and load of three joints in the loading process. Displacement control mechanism was applied at the free end of the beam by the MTS actuator in the whole loading process. Loading scheme (a) is applied for PC1, as shown in Figure 5(a). Due to the asymmetric design of the connection, it is observed that the structural response of PC1 was asymmetric in the experiment. This means that the positive bearing capacity of the joint is larger than the negative one. The use of steel plates attached to both sides of the cantilever beam is one major reason for the asymmetric responses. In order to avoid the early failure in the negative loading, there is another loading scheme (b) for PC2 and

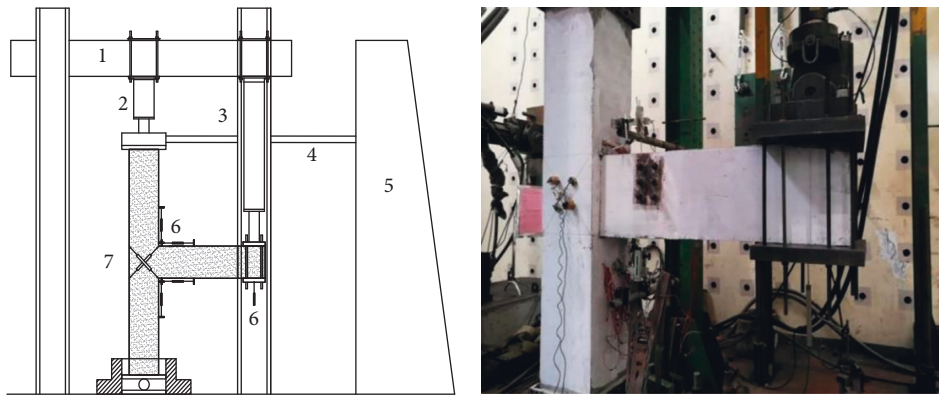

Figure 4: Experimental setup. (a) Schematic diagram (1, reaction beam; 2, jack; 3, actuator; 4, horizontal bracing; 5, reaction wall; 6, displacement meter; 7, extensometer). (b) Photo.

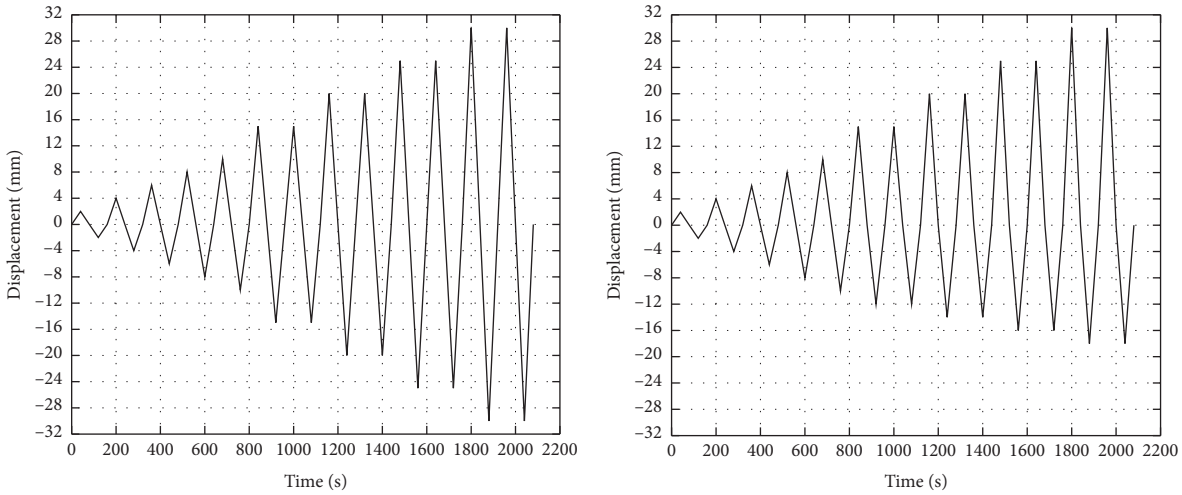

Figure 5: Loading scheme. (a) Loading cycles for PC1. (b) Loading cycles for PC2 and PC3.

PC3 (Figure 5(b)) in the later tests. In loading scheme (b), the maximum loading displacement of the negative direction is smaller than the positive loading displacement. In the elastic stage, one loading cycle is performed for each displacement step. With the test continuing, two full loading cycles are applied at the constant increment of 5 mm.

3. Experimental Results and Analysis

3.1. Experiment Phenomena. There is little difference in the crack pattern and the failure mode of all three joints, as shown in Figure 6. The joints PC1 and PC2 failed suddenly due to the steel bar bond slip in the connection area and significant concrete crushing, whereas joint PC3 kept perfect ductile deformation after the yielding of the longitudinal reinforcement. Welded rebars at the bottom of the beam in the joints PC1 and PC2 were fractured during the cyclic loading. This is due to the fact that the connection position of joints PC1 and PC2 coincides with the plastic hinge zone and the inelastic deformation of joints mainly concentrates on the plastic hinge zone. As a result, the deformation in the connection area of joints PC1 and PC2 is so large that the early connection failure of welded rebars occurred. However, the welded rebars of joint PC3 were not fractured and showed obvious yielding stage.

For the joint PC1, when the imposed displacement at the beam end achieved ±4 mm, the first crack appeared at a distance of 100 mm away from the column edge. With the displacement increasing to ±10 mm, several tiny shear cracks appeared around the steel plate and then extended to the bottom of the new-old concrete interface. The size and the number of these cracks continued to grow during the test until the spacing of the diagonal shear crack grew up to 10 mm on the bottom of the U-shaped groove at the displacement of ±30 mm. After that, the welded steel bars disconnected under the cyclic loading. At this time, the shear and the moment were transmitted depending on high-strength bolts and the strut-and-tie model in the corbel area, and then the concrete at the bottom of the U-shaped groove was divided into small oblique blocks in the direction of the struts.

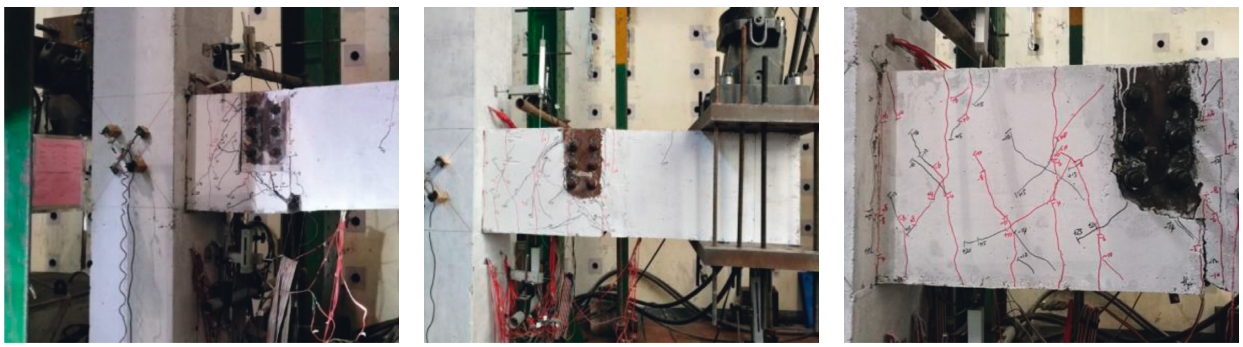

(a) (b) (c)

Figure 6: Crack distribution of (a) PC1, (b) PC2, and (c) PC3.

According to the test results of joint PC1, it is found that the structural response was unsymmetrical in the positive and negative direction. Hence, the improved loading scheme (b) in Figure 5(b) was adopted in the loading process of joints PC2 and PC3. From the test on the joint PC2, it was observed that the first cracking occurred at the displacement of +2 mm, also in some cases initiating from the bottom of the cantilever beam. With the load displacement increasing, obvious flexural cracks were concentrated in the connection zone, which can prevent excessive flexural cracks from extending to the column edge. Many diagonal cracks occurred at the loading displacement of ±8 mm, starting from the new-to-old concrete interface and then propagating toward the compression zone of the new-to-old concrete interface. At this stage, a series of concrete struts may be formed in the corbel. During the sequential loading cycles, more shear cracks with increasing width appeared at the bottom of the beam in the connection zone until the concrete was crushed and steel bars were exposed at the displacement of −25 mm. At the end of the test, the significant diagonal crack which initiated from the bottom of the U-shaped groove penetrated transversely through the whole beam section, resulting in significant concrete separation.

The final failure mode of joint PC3 was different from that of joints PC1 and PC2. In the initial loading stage, the first flexural crack appeared at the new-to-old concrete interface at the displacement of +4 mm. After that, more flexural cracks developed and extended along the beam to shear spans until some flexural cracks coincided with shear cracks. After the yielding of the main longitudinal steel bar, the diagonal cracks propagated rapidly and the concrete at the bottom of the beam was crushed significantly.

In general, the largest damage can be observed in the specimen PC1, followed by the specimens PC2 and PC3, which displayed a reduced number of cracks in the connection zone. The maximum shear crack width at the bottom of the beam in three joints was 8 mm, 6 mm, and 5 mm, respectively. As for specimens PC1 and PC2, the connection position is 450 mm and 600 mm away from the column edge, thus coinciding with the inherent plastic hinge zone. The plastic hinge of precast joints is formed at a distance of about 1.0–1.3 times the height of the beam away from the column edge. Thus, the connection position of joint PC1 is the most disadvantageous position under the cyclic loading and the weakest part in the whole structure. The rotation of the plastic hinge in the joint PC1 can enhance the deformation of the beam, which resulted in the widest crack. However, the connection position of joint PC3 is designed to be 750 mm away from the column edge so as to avoid coinciding with the plastic hinge region. As a result, the joint PC3 exhibited better mechanical properties, which had both higher strength and ductility.

It is worth noting that the cracks in the specimens were mainly concentrated in the connection zone, which can help to prevent the development of excessive cracks in the joint. It can thus be concluded that the plastic hinge was confined to the beam successfully by relocating the connection position to midspan of the beam. It can also be found that there were some cracks initiating from the column edge and then extending along with the beam longitudinal bars, which can be explained by the bond slip of steel bars under the cyclic loading.

3.2. Load-Displacement Hysteresis Curve. Figure 7 shows the hysteresis curves of specimens PC1, PC2, and PC3. It is obvious that the curve shape is unsymmetrical both in the positive and negative condition, which can be explained by enforcement effects of steel plates attached to both sides of the cantilever beam. At the elastic stage, the relationship between lateral load and displacement is linear. With the lateral load increasing, some steel bars begin to yield and the slope of the hysteresis loops decreases slowly due to the crack development. After reaching the peak load, the significant degradation in strength is observed in the joints PC1 and PC2, which can be attributed to the early connection failure of longitudinal steel bars in the connection zone under the cyclic loading, but the load-displacement curve of joint PC3 remains pretty stable. The hysteresis loops of joints PC1 and PC2 in the loading cycles are more pinched and show greater stiffness degradation as compared to joint PC3 which has larger hysteresis loops and reveals higher energy dissipation capacity. This is because significant concrete spalling occurs in the plastic hinge zone in the specimens PC1 and PC2. However, the connection position of PC3 does not coincide

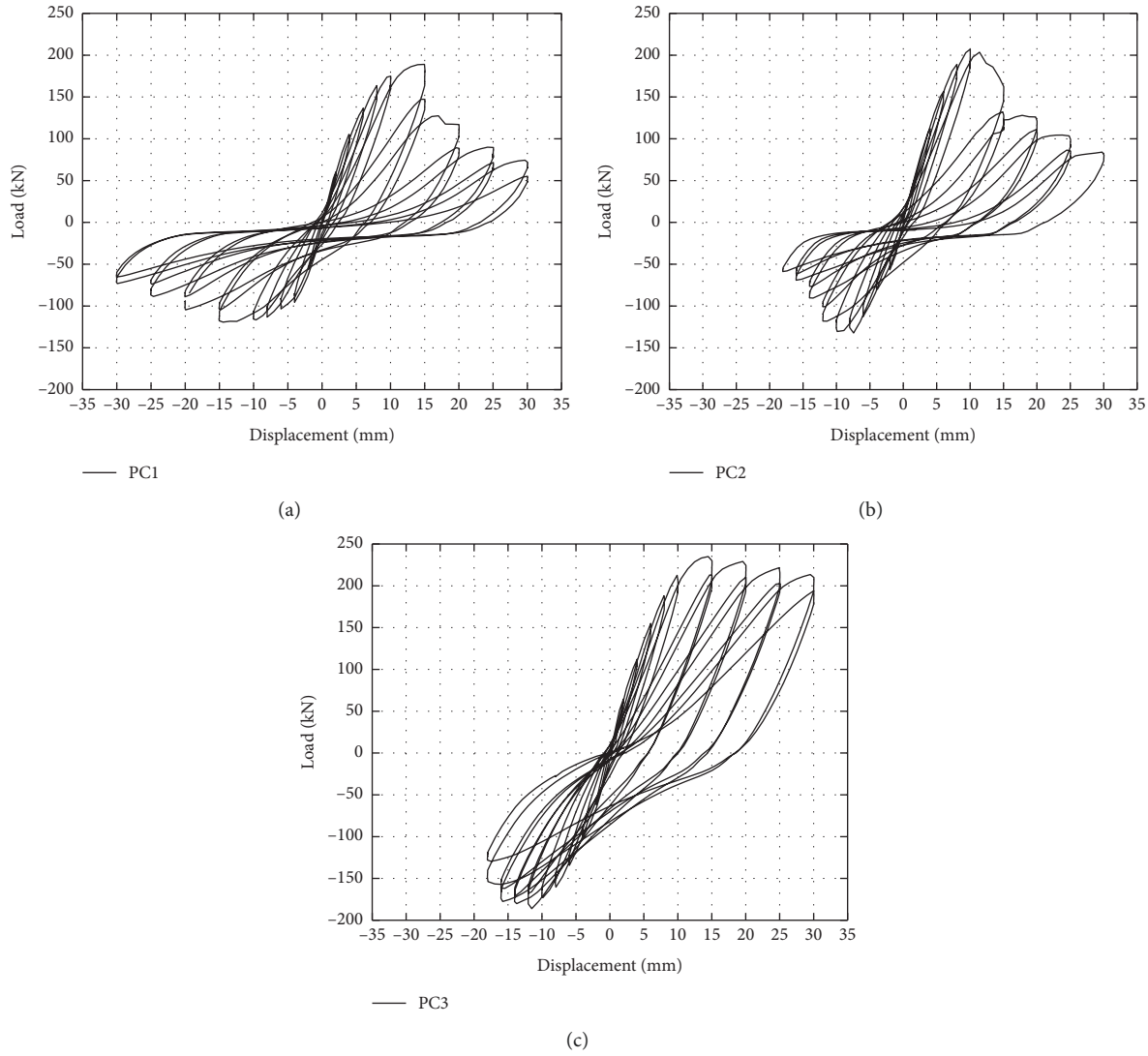

Figure 7: Hysteresis curves of the specimens. (a) PC1. (b) PC2. (c) PC3.

with the plastic hinge zone; hence, the damage of the beam is reduced. It can also be found that the peak load of the second cycle is smaller than that of the first cycle, which can be explained by the stiffness degradation due to the material damage. The trend is particularly noticeable in the specimens PC1 and PC2 which suffer more significant concrete crushing in the connection area.

3.3. Energy Dissipation Capacity. The energy dissipation capacity can be used to describe the ductile behaviour of structures. It can be measured based on the area circled by the hysteretic loop. For the curves with double cycles at the same displacement level, the average value of the area in two cycles is calculated as the energy dissipation coefficient according to the formulas provided in the *Test Code for Earthquake Resistant Building* (JGJ/T101-2015, 2015) [32]. The equivalent viscous damper ratio is also an important index to measure energy dissipation capacity, which can also be obtained from the hysteresis curve. As shown in Figure 8, the energy dissipation coefficient and the equivalent viscous damper ratio are calculated by the following equations:

$$E = \frac{S(\mathrm{ABC} + \mathrm{CDA})}{S(\mathrm{OBE} + \mathrm{ODF})}, \tag{10}$$

$$\zeta_{\mathrm{eq}} = \frac{1}{2\Pi} \frac{S(\mathrm{ABC} + \mathrm{CDA})}{S(\mathrm{OBE} + \mathrm{ODF})}, \tag{11}$$

where E is the energy dissipation coefficient, ζ_{eq} is the equivalent viscous damper ratio, being the ratio of the dissipated energy of the hysteretic loop to the strain energy divided by the constant 2π, S (ABC + CDA) is the area of the hysteresis loop, and S (OBE + ODF) is the area of triangles OBE and ODF.

The energy dissipation coefficient E and the equivalent viscous damper ratio ζ_{eq} of three specimens are summarized in Table 1. For the joint PC1, a larger amount of energy is absorbed as compared to specimens PC2 and PC3 when the

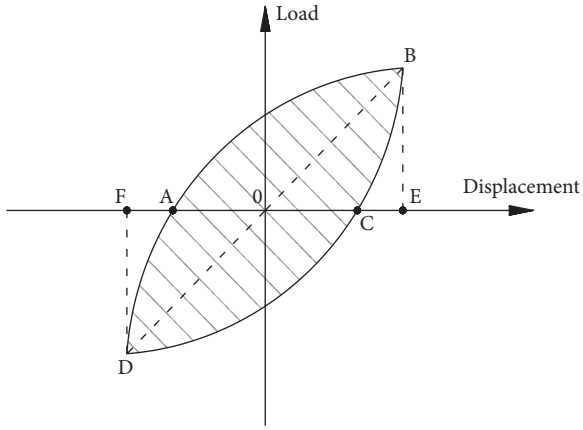

Figure 8: Calculation diagram.

loading displacement is less than 8 mm. The energy dissipation coefficient E of joint PC1 is 0.4765 larger than that of joints PC2 and PC3 of about 0.4462 and 0.3973, respectively. This is because the relocation of the plastic hinge increases the deformation capacity of the whole structure and leads to more cracks in the beginning loading. In fact, deformation and cracking provide a way to absorb energy; therefore, more cracks and deformation in the specimen PC1 contribute to higher energy dissipation capacity. The maximum energy dissipation coefficient E of joints PC1 and PC2 is obtained at the displacement of 20 mm and then decreases gradually, whereas the energy dissipation coefficient E of joint PC3 continues to increase until the end of the loading process. This can be attributed to the excessive deformation and significant concrete spalling in the joints PC1 and PC2, which result in significant reduction of the bearing capacity. The equivalent viscous damper ratio ζ_{eq} is used to describe the energy dissipation capacity during each cycle. The equivalent viscous damper ratio ζ_{eq} achieves the maximum of 0.1570 at the displacement of 20 mm for joint PC1, and the maximum value of 0.1686 is obtained at the displacement of 15 mm for joint PC2. After that, the equivalent viscous damper ratio ζ_{eq} decreases with the displacement increasing. The obvious inflection points imply that joints PC1 and PC2 have been severely damaged in the loading process. For joint PC3, its equivalent viscous damper ratio keeps rising and achieves 0.1530 at the displacement of 30 mm.

Figure 9 further compares the cumulative energy dissipation of three specimens, and similar conclusions can be drawn. At the elastic stage, there is no obvious difference in the cumulative energy dissipation capacity of test specimens. After the loading displacement increases to 15 mm, the cumulative energy dissipation capacity of joint PC3 exceeds that of joints PC1 and PC2. This is because some longitudinal steel bars in the joints PC1 and PC2 fracture and do not function effectively during the cyclic loading, whereas the reinforcement detailing in the connection zone of joint PC3 is still effective.

3.4. Skeleton Curve. The skeleton curves of all three joints can be obtained by picking up the ultimate load under each displacement level. The skeleton curves of three joints are also unsymmetrical, as shown in Figure 10. The upper steel plates anchored to both sides of the cantilever beam help to achieve larger strength in the positive direction. The critical data about skeleton curves are summarized in Table 2. The joint PC1 reaches the ultimate positive load of 188.68 kN at the displacement of +9.97 mm, and the negative load of 119.22 kN is obtained at the displacement of −8.40 mm (Figure 10(a)). The ultimate load of joint PC2 is slightly higher than that of joint PC1 with 207.13 kN at the displacement of +10.03 mm and 132.3 kN at the displacement of −7.44 mm (Figure 10(b)). The bearing capacity is mainly determined by steel bars; however, the longitudinal steel bars at the bottom of the beam in the joints PC1 and PC2 are disconnected earlier than the concrete crushing. Therefore, the bearing capacity of joint PC3 with integral bar connection under cyclic loads is the largest, and the ultimate load achieves 234.92 kN and 186.17 kN in the positive and negative direction, respectively. It can be seen that the skeleton curves of three joints are almost identical at the elastic stage which indicates that three joints achieve the similar initial stiffness. But with the cyclic load increasing, the stiffness begins to decline to some extent, which is mainly caused by the plastic damage of concrete and the yielding of steel bars. Considering significant concrete cracking of joints PC1 and PC2 before yielding of main longitudinal steel bars in the beam, the significant strength degradation of joints PC1 and PC2 can be observed in the sequential loading cycles. It is also found that there is no obvious yield platform except for joint PC3. This is because the yielding strength of beam steel bars is high, whereas the steel bar anchor system in the joints PC1 and PC2 fails before reaching yielding strength. The connection position of joints PC1 and PC2 coincides with the plastic hinge zone, and the inelastic deformation of joints mainly concentrates on the plastic hinge zone so that significant concrete spalling occurs in the plastic hinge zone in the beam of joints PC1 and PC2, but the connection position of joint PC3 does not coincide with the plastic hinge zone; hence, the damage of the beam is reduced.

3.5. Stiffness Degradation. The stiffness degradation can reflect the structural damage under earthquake loadings. When subjected to identical loading displacement level, the stiffness drops with the number of unloading-reloading cycles increasing. The average conversion value of the ring stiffness can be used to describe the stiffness degradation as shown in the following equation:

$$K = \frac{\sum_{i=1}^{n} P_j^i}{\sum_{i=1}^{n} \Delta_j^i}, \tag{12}$$

where $K$is the ring stiffness, $\Delta_j^i$is the displacement at the peak state of the i_{th} cycle at the j_{th} loading level, n is the cycle numbers ($n = 2$), and P_j^i is the maximal load of the i_{th} cycle at the j_{th} loading level. The stiffness degradation curves of three specimens are shown in Figure 11.

Table 1: Energy dissipation coefficient (E) and equivalent damping coefficient ratio ζ_{eq}.

Loading displacement (mm)	PC1		PC2		PC3	
	E	ζ_{eq}	E	ζ_{eq}	E	ζ_{eq}
6	0.4216	0.0731	0.3870	0.0619	0.3866	0.0616
8	0.4765	0.0759	0.4462	0.0710	0.3973	0.0633
10	0.5129	0.0817	0.5216	0.0831	0.4381	0.0698
15	0.8366	0.1332	0.8185	0.1686	0.7710	0.1228
20	0.9158	0.1570	0.9020	0.1500	0.8445	0.1345
25	0.7996	0.1273	0.8644	0.1376	0.8827	0.1406
30	0.7552	0.1203	0.6820	0.1086	0.9607	0.1530

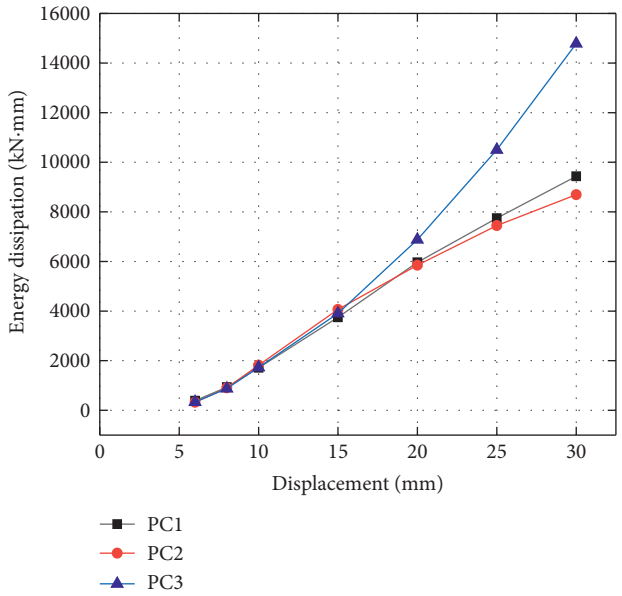

Figure 9: Comparison of cumulative energy dissipation.

For all three joints, the positive stiffness is larger than the negative one because of the enhancement effect of steel plates on both sides of the cantilever beam. The stiffness difference is more obvious after the cracking of the new-to-old concrete interface. All joints show sharp stiffness degradation in the initial displacement level, due to the development of cracks. With the displacement level increasing, the crack development slows down and the stiffness degradation tends to be stable. The positive stiffness of joint PC2 is larger than that of joint PC1 in the initial loading cycles but their stiffness degradation curves coincide with each other in the later loading cycles. The negative stiffness of joint PC2 drops faster than that of joint PC1 in the later loading cycles. The stiffness degradation of joints PC1 and PC2 is faster than that of joint PC3, which may be attributed to the early failure of the steel bar anchor system.

4. Numerical Model

Except for the test observations, finite element analyses are carried out to enable further understanding of behaviours of the dapped-end connection. The FE models P1, P2, and P3 are developed by ABAQUS software. FE models are established based on the actual conditions of the test such as boundary conditions and loading patterns as shown in Figure 12(a). The concrete plasticity damage is considered for both the column and beam so tensile cracking and compressive crushing can be exhibited in the model. All concrete members are modelled by tridimensional hexahedral solid element (C3D8R-type), and two-node linear 3D truss elements (T3D2-type) are used to model steel bars. The steel framework is embedded into the whole model, thus exhibiting no obvious steel bar bond slip. The contact interaction between the U-shaped groove and the corbel is introduced to define the assemblage effects. The dense mesh can improve the accuracy but would result in the excessive computed quantity; therefore, only steel plates and bolts adopt dense meshes. The finite element meshes of the joint are shown in Figure 12(b). The axial load is applied to the column which is set as pressure load, and the cyclic load is applied with inverse position from up and down. Bolt pretightening forces are applied in step to make sure the contact stability.

5. Comparison between Numerical and Experimental Results

Figure 13 shows the load-displacement curves of FE models. It can be seen that the hysteresis curves of numerical analyses for three joints P1, P2, and P3 are slightly different from those hysteresis curves measured in the experiment. The largest difference is that the hysteresis curves of experimental results show significant pinching, whereas the hysteresis curves of numerical results show less pinching, which can be attributed to the perfect bar bond behaviours in the numerical model. At the elastic stage, the stiffness of numerical responses for three joints is larger than experimental responses. This can be explained by the effect of pins in the practice, which are not ideal confines. After reaching the peak load, the experimental curves of joints PC1 and PC2 drop suddenly because of the connection failure of steel bars and significant concrete crushing, whereas the numerical curve just begins to drop gradually due to the plastic damage of concrete materials. But the numerical response of joint P3 is similar to the experimental response, still remaining stable after exceeding the peak load and showing the better energy dissipation capacity.

The comparison of skeleton curves is shown in Figure 14. It can be seen that the load-displacement envelops of numerical models show obvious yielding stage whether the connection position coincides with the plastic hinge zone or

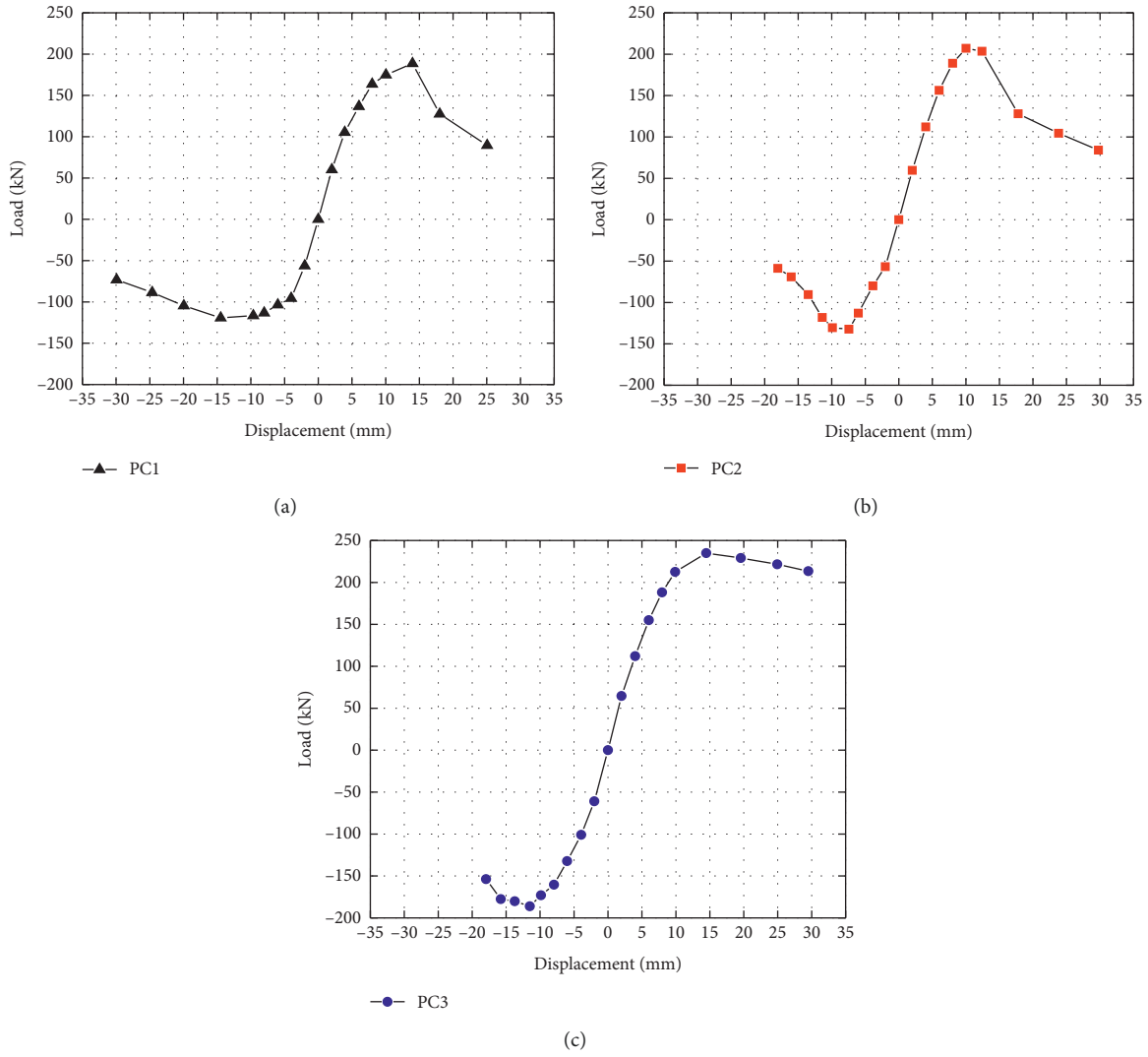

Figure 10: Skeleton curves of specimens. (a) PC1. (b) PC2. (c) PC3.

Table 2: Summary of results.

Specimen	Direction	Initial cracking		Yielding of main rebar		Ultimate state	
		Δ_{cr} (mm)	P_{cr} (kN)	Δ_y (mm)	P_y (kN)	Δ_u (mm)	P_u (kN)
PC1	Positive	4	64.45	7.58	166.95	9.97	188.68
	Negative	4	75.59	6.12	99.92	8.40	119.22
PC2	Positive	2	69.67	8.43	192.27	10.03	207.13
	Negative	4	79.96	6.56	119.56	8.44	132.26
PC3	Positive	4	112.09	9.75	208.49	14.47	234.92
	Negative	4	100.91	8.48	163.92	11.50	186.17

not. This is because the steel bars are merged as a whole steel frame and then embedded into the concrete, thus showing the perfect bond properties. As a result, three FE models do not fail suddenly due to the disconnected anchor system, and they keep perfect ductility capacity after the yielding of longitudinal steel bars.

6. Connection Position Effect

The connection position is the main variable that has a significant influence on the behaviours of dapped-end beam to column joints. In the experimental work, the connection position is designed to be 450 mm, 600 mm,

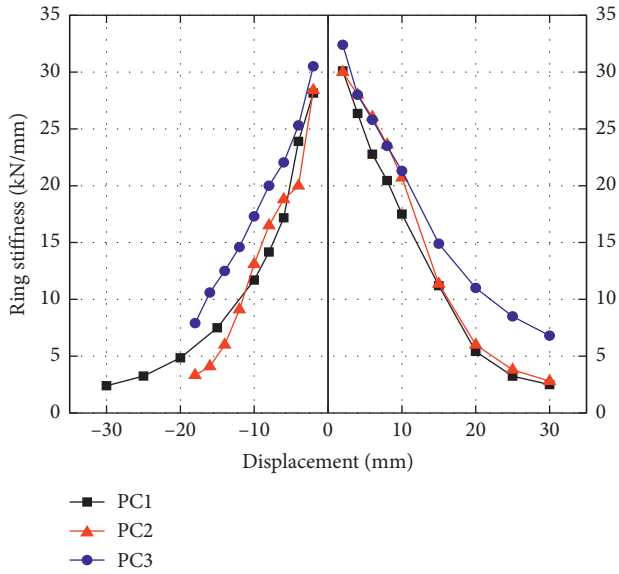

Figure 11: Ring stiffness-displacement curves.

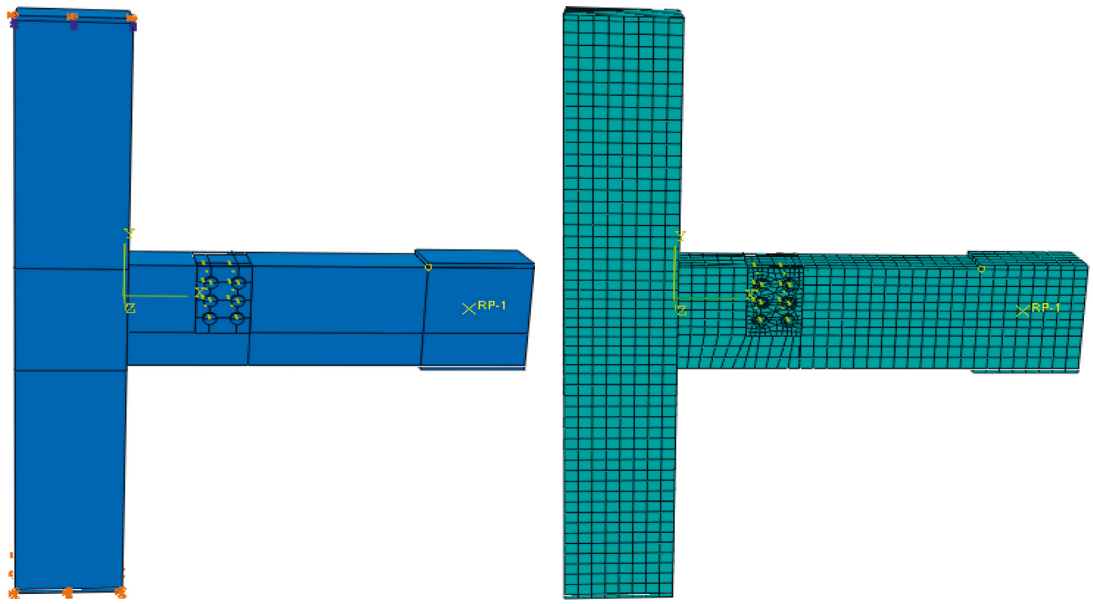

(a) (b)

Figure 12: (a) Boundary conditions. (b) Meshes of FE models.

and 750 mm away from the column edge. The experimental results can confirm the reliability of the FE model based on the fact that numerical analysis results can basically agree with the experimental results. In order to further understand the effects of connection position on the structural behaviours, FE models P4 and P5 are supplemented and the parameter setting is similar to joints P1, P2, and P3. The connection position of P4 and P5 is designed to be 900 mm and 1050 mm away from the column edge, respectively. Figures 15 and 16 show the hysteresis curves and skeleton curves of FE models. The connection position of joints P1 and P2 is within the plastic hinge zone, whereas for joints P3, P4, and P5, the connection position is relocated to a distance of 750 mm, 900 mm, and 1050 mm away from the column edge, thus not coinciding with the plastic hinge zone. The inelastic deformation of joints mainly occurred in the plastic hinge zone, so the deformation in the connection area of joints P1 and P2 is larger than that of other parts, which results in the early connection failure. After reaching the peak load, the bearing capacity of P1 and P2 decreases gradually. The maximum load of P1 and P2 is 197.94 kN and 190.71 kN, smaller than that of P3, P4, and

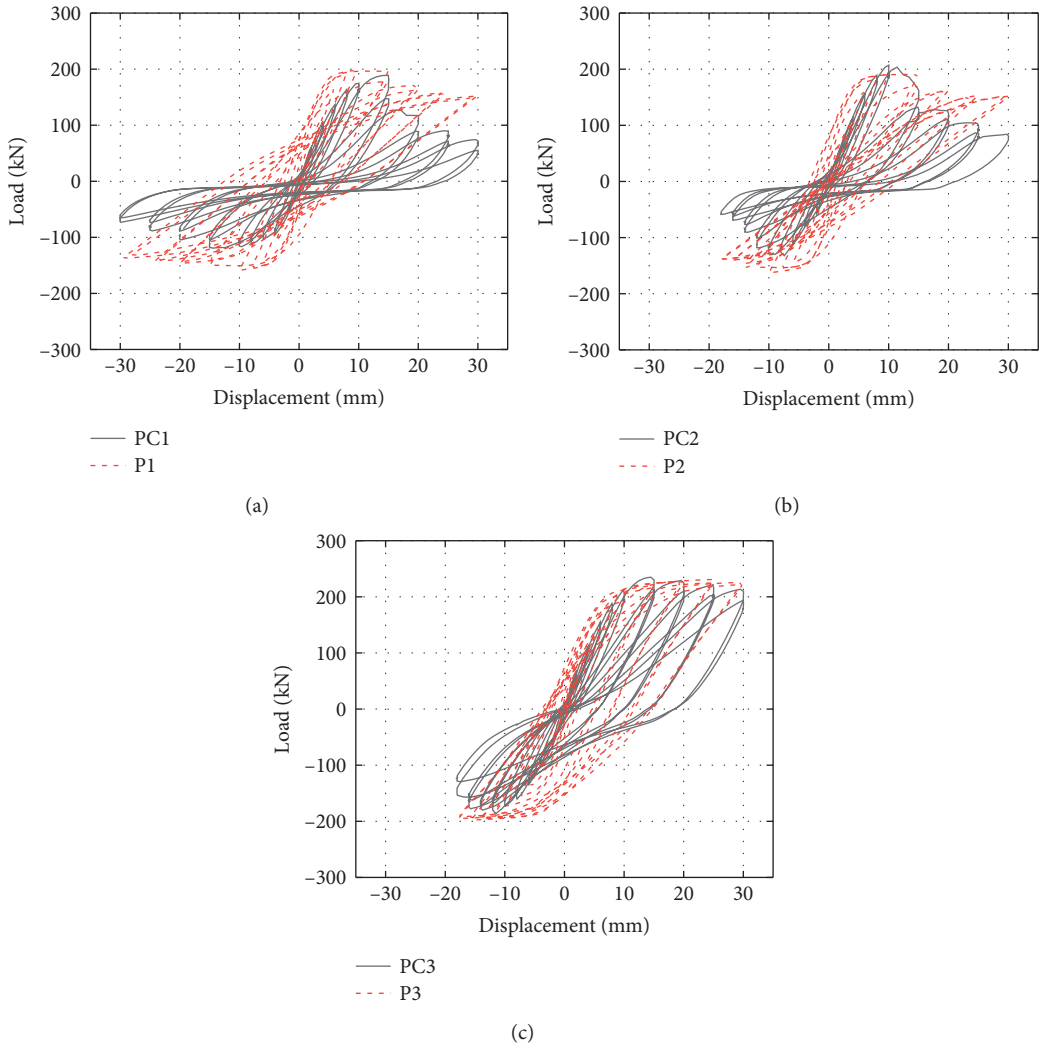

Figure 13: Comparison of hysteresis curves between numerical analyses and experimental results.

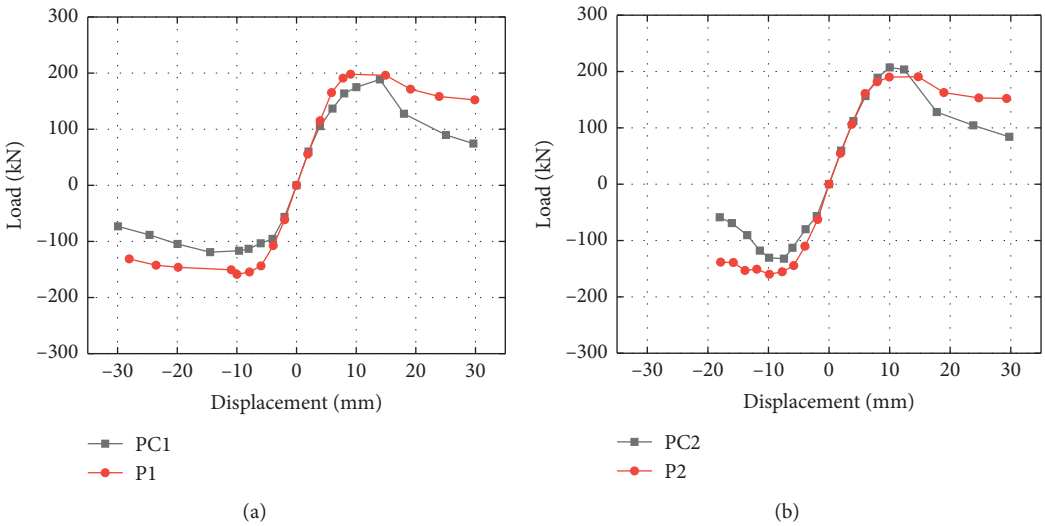

Figure 14: Continued.

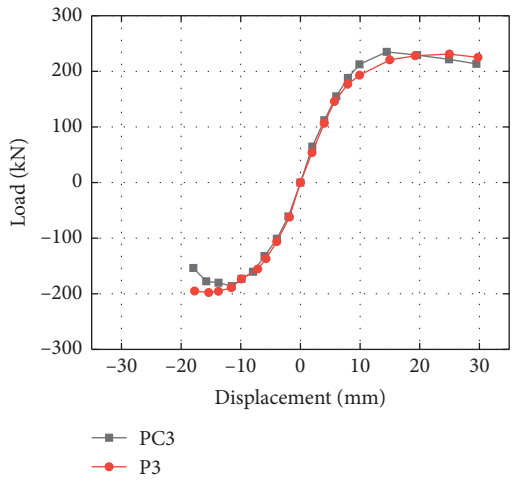

(c)

Figure 14: Comparison of skeleton curves between numerical analyses and experimental results.

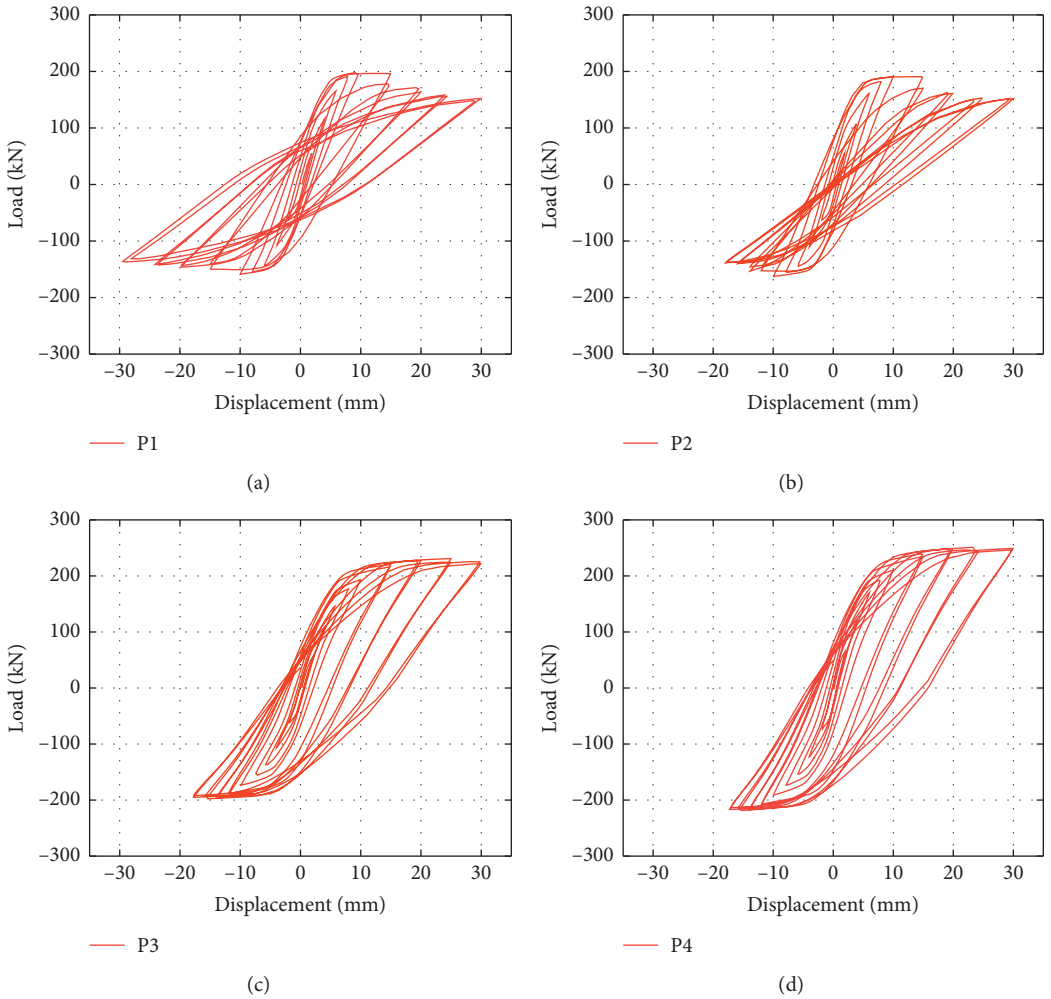

Figure 15: Continued.

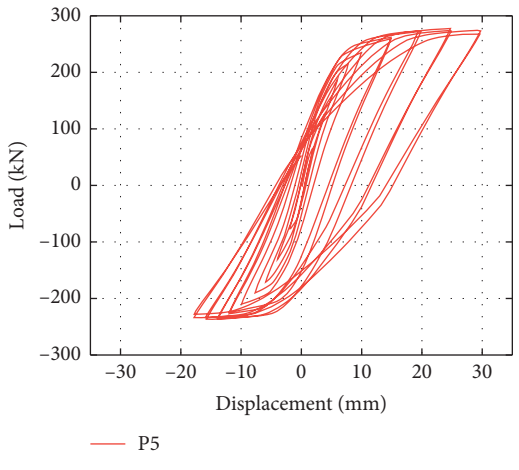

(e)

Figure 15: Hysteresis curves of numerical models.

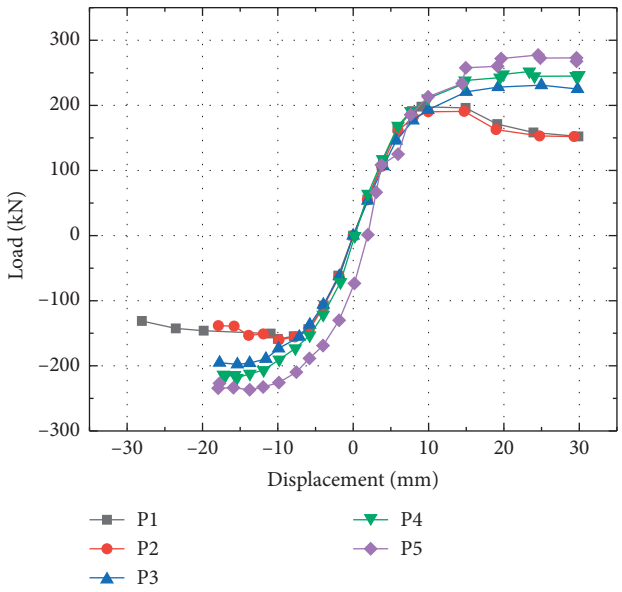

Figure 16: Skeleton curves of numerical models.

P5. Both the hysteresis curves of P1 and P2 exhibit significant pinching in the cyclic loading, which reveals that more significant bar bond slip and concrete crushing appear in the joints P1 and P2. As for joints P3, P4, and P5, the connection position is far away from the plastic hinge zone. They show similar cyclic responses, and the spindle-shaped hysteresis loops reveal that joints P3, P4, and P5 have good energy dissipation capacity. With the connection moving away from the plastic hinge zone, the peak load of joints P3, P4, and P5 is 231.06 kN, 251.95 kN, and 277.42 kN, respectively. This occurs due to the fact that the connection position does not coincide with the inherent plastic hinge zone and the connection position of joints P4 and P5 is also not in the midspan of the beam. As a result, the bearing capacity of joints P4 and P5 is slightly larger than that of P3.

7. Conclusions

In this paper, a new type of dapped-end beam to column connection is proposed, which can provide integrity for the joint and help to achieve the strong-column weak-beam and strong-joint weak member failure mechanism. The quasi-static tests were carried out to analyze the influence of the connection location on structural responses and mechanical properties. Based on the test results, FE analyses were carried out to further understand behaviours of the dapped-end connection. The major conclusions obtained are as follows.

Comparing the failure mode of three specimens in the test, the damage was mainly concentrated in the connection area. This means that the connection is the weakest part in the whole structural system. Because the connection is constructed away from the beam to column junction, the plastic hinge is relocated from the column edge to beam span, which could effectively protect the joint core area. During the whole loading process, there were few cracks in the joint core area and the column, so strong-joint weak-component and strong-column weak-beam principles can be achieved. After the new-old concrete interface cracking, the high-strength bolts and the strut-to-tie model were used to act as force transfer mechanism. The bolts performed very well in the whole loading process and provided good friction and tight force for joints after the disconnection of longitudinal steel bars of PC1 and PC2.

The positive bearing capacity of three test specimens was larger than that of the negative bearing capacity which can be attributed to the strengthening method (two steel plates on both sides of the U-shaped groove). The bearing capacity and the energy dissipation capacity of PC3 had more advantages than that of PC1 and PC2. In fact, the plastic hinge of precast joints is formed at a distance of about 1.0–1.3 times the height of the beam away from the column edge. Therefore, the plastic hinge zone of PC1 and PC2 is relocated to the connection area, the weakest part of the beam. However, the plastic hinge zone of PC3 is positioned in the area away from

the connection part. As a result, the plastic hinge rotation of PC1 and PC2 was larger than that of PC3, which resulted in the excessive deformation of the beam and the large strength reduction.

From the comparison between the finite element analysis results and the experimental results, it is found that the numerical results can agree with experimental results, but little difference can be observed in the specimens P1 and P2, which can be explained by the effects of steel bar bond slip at the bottom of the beam. This means that the overall reliability of numerical models can be verified.

In order to further study the effects of the connection position on the structural behaviours, FE models P4 and P5 were supplemented based on the comparison results between experimental responses and numerical analyses. It is found the cyclic response of P3, P4, and P5 was similar, but the bearing capacity of P4 and P5 was larger. This can be attributed to effects of connection position, which neither coincides with the plastic hinge zone nor coincides with the midspan part.

When the connection is constructed in the beam-column junction, joints would not only be subjected to large amounts of internal forces but also have difficulties in construction technology due to the heavily congested reinforcement in the joint core area. However, relocating the connection to the beam span can achieve the minimal amount of forces and deal with worry about the construction quality. Also, the connection relocation can help to restrain diagonal cracking in the joint and achieve beam hinge mechanism. The major inelastic deformation appears in the connection area and the plastic hinge zone so that the strong-joint weak-component and strong-column weak-beam mechanisms can be achieved.

Data Availability

The data used to support the findings of the study are included in the article.

Conflicts of Interest

The authors declare there are no conflicts of interest regarding the publication of the paper.

Acknowledgments

The authors are grateful for the financial support provided by the National Natural Science Foundation of China (nos. 51578159, 51678158, 51878181, and 51608128), the Program for New Century Excellent Talents at Fujian Province University (2016, no. 83016017), the Cooperative Project of Fujian Province Colleges and Universities (no. 2016H6011), the Natural Science Foundation of Fujian Province (no. 2018J01773), and the Cooperative Leading Project of Fujian Province Colleges and Universities (no. 2017H0016).

References

[1] H. Wang, E. M. Marino, P. Pan, H. Liu, and X. Nie, "Experimental study of a novel precast prestressed reinforced concrete beam-to-column joint," *Engineering Structures*, vol. 156, pp. 68–81, 2018.

[2] G. Santarsiero and A. Masi, "Seismic performance of RC beam-column joints retrofitted with steel dissipation jackets," *Engineering Structures*, vol. 85, pp. 95–106, 2015.

[3] H. Parastesh, I. Hajirasouliha, and R. Ramezani, "A new ductile moment-resisting connection for precast concrete frames in seismic regions: an experimental investigation," *Engineering Structures*, vol. 70, pp. 144–157, 2014.

[4] J. I. Resreepo and P. Robert, "Design of connections of earthquake resisting precast reinforced concrete perimeter frames," *PCI Journal*, vol. 40, no. 5, pp. 68–76, 1995.

[5] M. J. N. Priestley and J. R. Tao, "Seismic response of precast prestressed concrete frames with partially debonded tendons," *PCI Journal*, vol. 38, no. 1, pp. 58–69, 1993.

[6] M. J. N. Priestley and G. A. Macrae, "Seismic tests of precast beam-to-column joint subassemblages with unbonded tendons," *PCI Journal*, vol. 41, no. 1, pp. 64–81, 1996.

[7] M. Priestley, S. Sritharan, J. R. Conley, and S. S. Pampanin, "Preliminary results and conclusions from the press five story precast concrete test building," *PCI Journal*, vol. 44, no. 6, pp. 42–66, 1999.

[8] B. G. Morgen and Y. C. Kurama, "Seismic Design of friction-damped precast concrete frame structures," *Journal of Structural Engineering*, vol. 133, no. 11, pp. 1501–1511, 2007.

[9] X. Lu, Y. Cui, J. Liu, and W. Gao, "Shaking table test and numerical simulation of a 1/2-scale self-centering reinforced concrete frame," *Earthquake Engineering & Structural Dynamics*, vol. 44, no. 12, pp. 1899–1917, 2015.

[10] F. Sarti, T. Smith, S. Pampanin et al., "Experimental and analytical study of replaceable buckling-restrained fused-type (BRF) mild steel dissipaters," in *Proceedings of the New Zealand Society for Earthquake Engineering Annual Conference*, Wellington, New Zealand, April 2013.

[11] D. Guan, Z. Guo, Q. Xiao, and Y. Zheng, "Experimental study of a new beam-to-column connection for precast concrete frames under reversal cyclic loading," *Advances in Structural Engineering*, vol. 19, no. 3, pp. 529–545, 2016.

[12] H. J. Im, H. G. Park, and T. S. Eom, "Cyclic loading test for reinforced-concrete-emulated beam-column connection of precast concrete moment frame," *ACI Structural Journal*, vol. 110, no. 1, pp. 115–126, 2013.

[13] S. H. Kim, J. H. Moon, and L. H. Lee, "An experimental study of the structural behaviour on the precast concrete beam-column interior joint with splice type reinforcing bars," *Journal of the Architectural Institute of Korea Structure & Construction*, vol. 20, no. 10, pp. 53–61, 2004.

[14] H. K. Chio, Y. C. Chio, and C. S. Chio, "Development and testing of precast concrete beam-to-column connections," *Engineering Structures*, vol. 56, pp. 1820–1835, 2013.

[15] S. Pampanin, C. Christopoulos, and T. Chen, "Development and validation of a metallic haunch seismic retrofit solution for existing under-designed RC frame buildings," *Earthquake Engineering*, vol. 16, no. 1, pp. 21–42, 2006.

[16] A. Pimanmas and P. Chaimahawan, "Shear strength of beam-column joint with enlarged joint area," *Engineering Structures*, vol. 32, no. 9, pp. 2529–2545, 2010.

[17] T. S. Eom, H. G. Park, H. J. Hwang et al., "Plastic hinge relocation methods for emulative PC beam-column connections," *Journal of Structural Engineering*, vol. 142, no. 2, pp. 1–13, 2016.

[18] C.-C. Chen, C.-C. Lin, and C.-H. Lin, "Ductile moment connections used in steel column-tree moment-resisting

frames," *Journal of Constructional Steel Research*, vol. 62, no. 8, pp. 793–801, 2006.

[19] O. Arowojolu, A. Ibrahim, M. K. Rahman, M. Al-Osta, and A. H. Al-Gadhib, "Plastic hinge relocation in reinforced concrete beam-column joint using carbon fiber-reinforced polymer," *Advances in Structural Engineering*, vol. 22, no. 14, pp. 2951–2965, 2019.

[20] J. H. Khoo, B. Li, and W. K. Yip, "Tests on precast concrete frames with connections constructed away from column faces," *ACI Structural Journal*, vol. 103, no. 1, pp. 18–27, 2006.

[21] A. A. Astaneh, *Seismic Design of Steel Column-Tree Moment-Resisting Frames*, Structural Steel Educational Council, Moraga, CA, USA, 1997.

[22] D. D. Joshi and P. V. Patel, "Experimental study of precast dry connections constructed away from beam-column junction under progressive collapse scenario," *Asian Journal of Civil Engineering*, vol. 20, no. 2, pp. 209–222, 2019.

[23] C. W. French, O. Amu, and C. Tarzikhan, "Connections between precast elements-failure outside connection region," *Journal of Structural Engineering*, vol. 115, no. 2, pp. 316–340, 1989.

[24] C. W. French, M. Hafner, and V. Jayashankar, "Connections between precast elements-failure within connection region," *Journal of Structural Engineering*, vol. 115, no. 12, pp. 3171–3192, 1989.

[25] M. Savoia, N. Buratti, and L. Vincenzi, "Damage and collapses in industrial precast buildings after the 2012 Emilia earthquake," *Engineering Structures*, vol. 137, pp. 162–180, 2017.

[26] C. E. Chalioris and K. E. Bantilas, "Shear strength of reinforced concrete beam-column joints with crossed inclined bars," *Engineering Structures*, vol. 140, pp. 241–255, 2017.

[27] F. Faleschini, L. Hofer, M. A. Zanini, M. dalla Benetta, and C. Pellegrino, "Experimental behavior of beam-column joints made with EAF concrete under cyclic loading," *Engineering Structures*, vol. 139, pp. 81–95, 2017.

[28] R. Park and D. K. Bull, "Seismic resistance of frames incorporating precast prestressed concrete beam shells," *PCI Journal*, vol. 31, no. 4, pp. 54–93, 1986.

[29] China Architecture Design Institute 15G310-1~2, *Construction of Assembled Concrete Connection Joints*, China Planning Press, Beijing, China, 2015, in Chinese.

[30] China Architecture Design Institute JGJ 1-2014, *Technical Specification for Assembled Concrete Structure*, China Architecture and Building Press, Beijing, China, 2014, in Chinese.

[31] ACI Committee318, *Building Code Requirements for Structural Concrete (ACI 318-02) and Commentary (ACI 318R-02)*, American Concrete Institute, Farmington Hills, MI, USA, 2001.

[32] China Academy of Building Research, *Test Code for Earthquake Resistant Building JGJ/T101-2015*, China Architecture and Building Press, Beijing, China, 2015, in Chinese.